Buoyancy Ratio Effect on Thermosolutal Convective Transitions in a Very Narrow Porous Annulus

A. Ja[1], A. Cheddadi[1]

[1]. Research Team "Thermal Systems and Real Flows", Mohammadia School of Engineers, Mohammed V University in Rabat, cheddadi@emi.ac.ma

Abstract

This work presents a numerical investigation of the natural thermosolutal convection in a very narrow horizontal annular cylinder filled with a porous medium saturated by a binary fluid. The governing equations describing the two-dimensional steady state flow are solved by an Alternating Direction Implicit scheme (ADI). In the objective to study the effect of the buoyancy ratio, $-42 \le N \le 34$, on flow structure and heat and solutal transfer rates, in a cavity of radius ratio R = 1.1, a fixed Rayleigh number, Ra = 50, and Lewis number, Le = 2, values are adopted. Critical buoyancy ratio values are determined for different flow structures. The obtained results show that complex multicellular flows appear when increasing the N value respectively in the cooperating and opposite cases.

Keywords: *Thermosolutal convection, Porous medium, Narrow annular geometry, ADI, Critical buoyancy ratio.*

1. Introduction

The study of heat and mass transfer within porous media has been the subject of a large number of studies in recent decades, due to its numerous applications (thermal insulation, heat exchangers...). Cavities of different geometries, such as the vertical annular cavities subject to horizontal temperature gradients, have been widely studied numerically and analytically [1]. Constant temperature and concentration imposed across the vertical walls [2] or opposing temperature and concentration gradients, were also studied numerically in this configuration [3]. Most of the existing works on natural convection in a horizontal annular porous media are concerned with the case of a cavity subject to temperature gradients [4], and the double-diffusive natural convection has been investigated with and without the Soret effect [5], [6].

In the present paper, the flow structure transitions in the case of thermosolutal convection will be studied in a very narrow horizontal annular cavity delimited by two coaxial, isotherm, impermeable cylinders, filled with a porous medium saturated by a binary fluid. The inner and outer cylinder of radius r_i and r_o are maintained at constant and uniform temperature and concentration (T_i, S_i) and (T_o, S_o) respectively with $T_i > T_o$ and $S_i > S_o$, as illustrated in Fig.1. The binary fluid was considered incompressible, Newtonian and satisfying the Boussinesq approximation. All the results are presented for a cavity of radius ratio R = 1.1.

2. Mathematical Formulation

The dimensionless steady state form of the governing equations describing the two-dimensional flow are Darcy's equation, conservation of energy and species equations, which are given in terms of stream function formulation as:

$$\nabla^2\psi = -Ra\left[\left(\sin\varphi\frac{\partial T}{\partial r}+\frac{\cos\varphi}{r}\frac{\partial T}{\partial\varphi}\right)+N\left(\sin\varphi\frac{\partial S}{\partial r}+\frac{\cos\varphi}{r}\frac{\partial S}{\partial\varphi}\right)\right] \quad (1)$$

$$\left(\vec{V}.\nabla\right)T=\nabla^2 T \quad (2)$$

$$\left(\vec{V}.\nabla\right)S=Le^{-1}\nabla^2 S \quad (3)$$

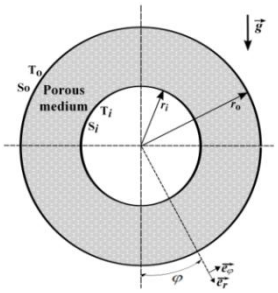

FIGURE 1. Schematic diagram of annular domain.

Where T and S are respectively the dimensionless temperature and concentration, the stream function Ψ is defined by $u=\frac{1}{r}\frac{\partial\psi}{\partial\varphi}$ and $v=-\frac{\partial\psi}{\partial r}$, where u and v are respectively the radial and tangential velocity components. The thermal and solutal transfer rates can be expressed in terms of the average Nusselt number, $\overline{Nu}$, and average Sherwood number, $\overline{Sh}$, defined respectively by the following expressions: $\overline{Nu}=-\frac{1}{\pi}LnR\int_0^\pi\left.\frac{\partial T}{\partial r}\right|_{r=1}d\varphi$ and $\overline{Sh}=-\frac{1}{\pi}LnR\int_0^\pi\left.\frac{\partial S}{\partial r}\right|_{r=1}d\varphi$.

The three dimensionless numbers that appear in the governing equations are defined by:

$$Ra=\frac{g\beta_T\Delta TKr_i}{\nu\alpha},\quad N=\frac{\beta_S\Delta S}{\beta_T\Delta T},\quad Le=\frac{\alpha}{D}.$$

The boundary conditions in dimensionless form are expressed as:

$$r = 1 : T = 1,\ S = 1 \text{ and } \frac{\partial\psi}{\partial\varphi} = 0,\ \forall\varphi \quad (4)$$

$$r = R : T = 0,\ S = 0 \text{ and } \frac{\partial\psi}{\partial\varphi} = 0,\ \forall\varphi \quad (5)$$

Taking into account the symmetry of the problem, two additional boundary conditions are introduced:

$$\varphi = 0,\pi : \frac{\partial T}{\partial\varphi} = 0,\ \frac{\partial S}{\partial\varphi} = 0 \text{ and } \frac{\partial\psi}{\partial r} = 0,\ \forall r \quad (6)$$

3. Numerical method

The governing dimensionless equations (1-3) are discretized using the centered Finite Difference method, with the Alternating Direction Implicit scheme (ADI). The Thomas Tridiagonal Matrix Algorithm is employed to resolve the algebraic systems. The iteration process was assumed to converge when the following criterion is satisfied in each node of the grid: $\frac{\chi_{i,j}^{n+1} - \chi_{i,j}^{n}}{\chi_{i,j}^{n}} \leq 10^{-8}$, χ refers to *T*, *S*, or Ψ, and the superscript *n* indicates the iteration number. The subscripts (*i*,*j*) represent the grid node. In a previous work [6], grid independence tests were carried out in the case of cooperation buoyancy forces, showing that a 91 x 111 (r, φ) mesh, is sufficiently fine to ensure an accurate steady solution. For the opposite buoyancy forces the same process is adopted and show that 101 x 141 mesh is optimal.

4. Results and discussion

4.1 Flow structure

Fig. 2 shows the flow patterns obtained for the opposite buoyancy forces, $-42 \leq N \leq 0$. To better visualize the flow structures, a section zoom $0 \leq \varphi \leq \frac{\pi}{2}$ is used.

Increasing the *N* value for the opposite buoyancy forces give rise to much complex flow structures. Firstly, the unicellular flow dominates over the interval [−5.2, 0] except the value $N = -1$. The range]−1, 0] is characterized by a counterclockwise cell (due to the thermal force domination) occupying the entire annular space. While the second range is characterized by the solutal force domination allowing the clockwise recirculation. Thus, a small increase in buoyancy ratio to the critical value $N_c = -5.21$ implies a first bifurcation from the unicellular to the bicellular flow characterized by a small counterclockwise cell, which appears in the bottom part of the cavity, where a high destabilizing solutal gradient occurs, as illustrated in Fig. 2.a. The clockwise cell undergoes a pinching with increasing the *N* value and allows to the onset of the bicellular swirling flow (see fig. 2.b). Furthermore, the corotative vortices separate at $N_c = -5.9$, becoming independent cells. Then, a new counterclockwise cell takes place between the two corotative cells and a new pinching of the main clockwise cell occurs, as shown in Fig. 2.c, giving rise to a tetracellular swirling flow. By the same process, the two corotative vortices separate and a new counterclockwise cell develops between them, which leads to the onset of an hexacellular flow (see Fig. 2.d). At the value $N_c = -14.2$, the last clockwise cell in the bottom part of the cavity crashes the counterclockwise one, situated below. At the same time as the main clockwise cell undergoes a new pinching, an heptacellular flow develops, as represented in Fig. 2.e. This flow pattern persists over the range $-17.9 \leq N \leq -14.2$. Moreover, a reverse transition is observed at $N_c = -18$, from the heptacellular to the pentacellular flow occurring over the large range $-42 \leq N \leq -18$, as illustrated in Fig. 2.f.

For the cooperation case, the same flow pattern discussed in the opposite buoyancy forces case, up to the hexacellular flow, remains. The range of each flow structure is plotted in Fig. 3. In this situation, the destabilizing thermal gradient effect strongly exceeds the stabilizing solutal one in the top part of the annular cavity, where the multicellular flow is observed (not shown here).

Beyond the value $N_c = 20.3$, a reverse transition is detected from the hexacellular to the tetracellular flow, this flow pattern persists over the entire range $20.3 \leq N \leq 34$.

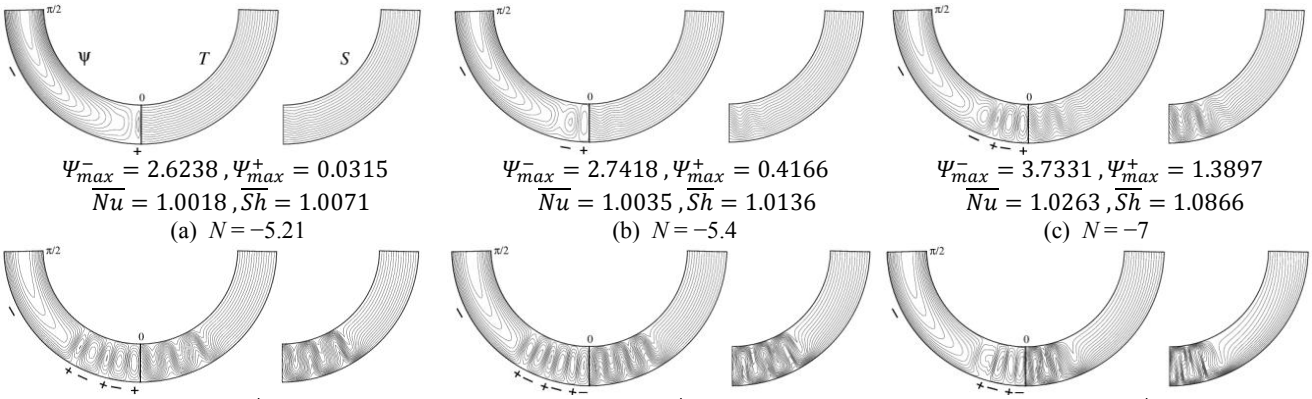

FIGURE 2: Flow structure behaviors, (a) bicellular, (b) tetracellular, (c) hexacellular, (d) heptacellular and (e) pentacellular for $Ra = 50$, $Le = 2$ and $R = 1.1$.

4.2 Flow intensity

Fig. 3 shows the variation of the flow intensity, Ψ, as function of the buoyancy ratio for both cases (i.e. cooperation and opposite). The Ψ_{max}^{-} (resp. Ψ_{max}^{+}) depicted, corresponds to the maximum clockwise flow intensity (resp. counterclockwise) recirculation. For the unicellular flow $-5.24 \leq N \leq 4.61$, the Ψ_{max}^{-} (resp. Ψ_{max}^{+}) in opposite (resp. cooperation) case increases progressively with increasing *N* values. The gradual increase in the *N* value leads to a progressive increase in Ψ_{max}^{-} and Ψ_{max}^{+} for the bicellular, tetracellular and hexacellular flows. At the critical value $N_c = -14.2$, the flow transits from hexacellular to heptacellular flow,

involving a significant decrease in Ψ_{max}^{-} (−12.4%), due to the reduction in the size of the clockwise cells. Beyond this critical value, the development of the clockwise cells leads to an enhancement of Ψ_{max}^{-}.

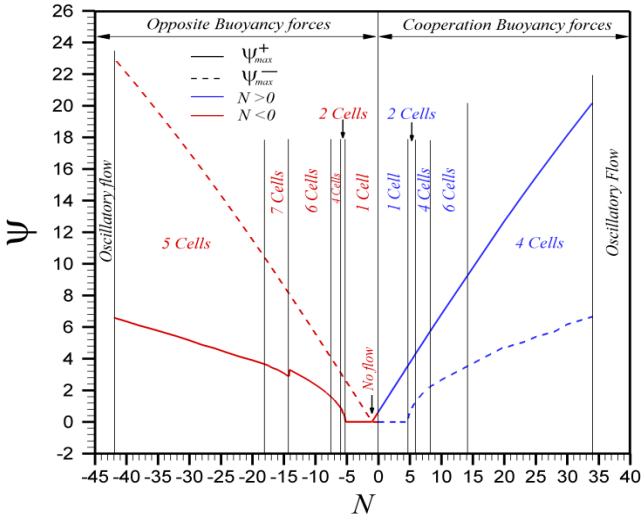

FIGURE 3: Flow intensity behavior as function of *N* values

Similar behaviors are observed for the cooperation case, where the intensity of the flow increases through the transition between different flow structures.

4.3 Heat and mass transfer rates

Fig. 4 shows the variation of the overall Nusselt, $\overline{Nu}$, and Sherwood, $\overline{Sh}$, numbers as a function of buoyancy ratio. The values of $\overline{Nu}$ and $\overline{Sh}$ presented for the unicellular flow are almost of the order of unity for both *N* cases. It is therefore concluded that for very narrow annular cavities and for values |N| ≤ N_c, both transfer rates are dominated by conduction / diffusion for both cases.

The transition to the multicellular flows, as discussed above, is characterized by the creation and development of convective cells, given the direct transport of particles through the contact zone of the counter-rotating cells, which improves $\overline{Nu}$ and $\overline{Sh}$. The shape of the isotherms and isoconcentration lines shown in Fig. 2 illustrates a strong distortion in the bottom part of the cavity for $N \leq 0$. Conversely, at the upper part of the cavity for $N \geq 0$. This allows concluding that the influence of the buoyancy ratio on the thermal and solutal distribution in the narrow cavity is remarkable when increasing *N* value, and hence, a progressive increase of $\overline{Nu}$ and $\overline{Sh}$ is observed. At the critical value N_c = −14.2, the transition from the hexacellular to heptacellular flow allows a small increase of $\overline{Nu}$ and $\overline{Sh}$, 1.17% and 2.08%, respectively. Thus the reverse transition from the heptacellular to pentacellular flow causes a reduction of the number of convective cells, involving a reduction of $\overline{Nu}$ and $\overline{Sh}$, −2.95% and −4.93% respectively. After this, the development of the convective cells size causes a gradual increase of $\overline{Nu}$ and $\overline{Sh}$. The same remarks are observed for $N \geq 0$, where the bifurcation from tetracellular to hexacellular flow (N_c = 8.1) is characterized by the increasing of $\overline{Nu}$ and $\overline{Sh}$, 2.07% and 5.28% respectively. However, the shift from hexacellular to tetracellular (N_c =20.3) reduces $\overline{Nu}$ and $\overline{Sh}$, −5.32% and −7.72%, respectively.

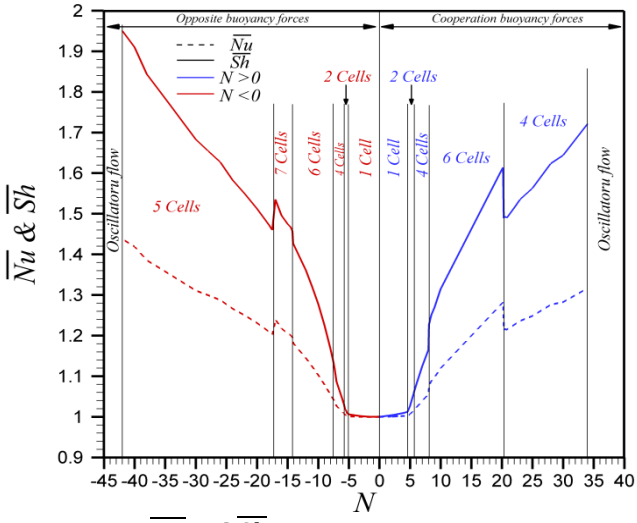

FIGURE 4: $\overline{Nu}$ and $\overline{Sh}$ behaviors as function of *N* values

5. Conclusion

A numerical investigation of double-diffusive natural convection in a horizontal porous annulus saturated with a binary fluid using the ADI method is presented. Results are given for the radius ratio *R* = 1.1 and Rayleigh number *Ra* = 50. The effect of the buoyancy ratio has been investigated. The variation of this parameter reveals its, especially, on the flow structure and on the rates of heat and mass transfer.

Reference

[1] F. Alavyoon, *On natural convection in vertical porous enclosures due to prescribed fluxes of heat and mass at the vertical boundaries*, Int. J. Heat Mass Transfer 36 (10) (1993) 2479-2498.

[2] H. Beji, R. Bennacer and R. Duval, *Double-diffisive natural convection in a vertical porous annulus*, Num. Heat Transfer, part A, 36 (1999) 153-170.

[3] S. Chen, J. Tolke, and M. Krafczyk, *Numerical investigation of double-diffusive (natural) convection in vertical annuluses with opposing temperature and concentration gradients*, Int. J. Heat Fluid Flow , 31 (2010) 217-226.

[4] M. C. Charrier-Mojtabi, *Numerical simulation of two- and three dimensional free convection flows in a horizontal porous annulus using a pressure and temperature formulation*, Int. J. Heat Mass Transfer , 40 (7) (1997) 1521-1533.

[5] Z. Alloui, and P. Vasseur, *Natural convection in a horizontal Annular porous cavity saturated by a binary mixture*, Computational Thermal Sciences, 3 (5) (2011) 407-417.

[6] A. Ja, J. Belabid, A. Cheddadi, *Heat and mass transfer in a saturated porous medium confined in cylindrical annular*, International Journal of Mechanical, Aerospace, Industrial and Mechatronics Engineering, 9(4) (2015) 525-529.